

Radio imaging method (RIM) or diagnostic imaging of anomalous geologic structures in coal seam waveguides

L.G. Stolarczyk and R.C. Fry

Abstract—*In coal-bearing formations, seams are often bounded by sedimentary layers of mudstone, claystone or shale. When the electrical conductivity of the surrounding sediment layers is greater than the conductivity of the seam, a natural parallel-plate waveguide forms in the strata. For frequencies below the AM broadcast band, the waveguide can be used for the transmission of electromagnetic (EM) waves. In a uniform seam, the primary wave travels in the coal layer along paths between a radiating antenna and a distant receiving antenna. The travel distance increases with seam height and the conductivity of the surrounding sediment layers. The distance decreases with increased coal conductivity. In Cretaceous western bituminous coal, the distance may exceed 549 m (1800 ft).*

Anomalous geologic disturbance zones such as faults, shear zones, paleochannels, sills and dikes significantly alter the values of EM wave propagation constants (attenuation and phase) expected in a uniform seam. In the neighborhood of an anomaly, EM wave energy is scattered (reflected and diffracted). Scattering creates secondary waves in the seam waveguide.

A receiving antenna at a remote location in the coal seam can be used to measure the magnitude and phase of the EM wave at the end of the path. The measured data can be processed to determine the average value of the propagation constants along each path. Paths with anomalous propagation constants are used to locate and image geologic disturbance zones.

Radio Imaging Method (RIM) instrumentation, survey procedures and data processing (tomography) algorithms have been developed to image geologic structure in advance of mining. The survey is conducted between gate roads of a longwall panel. Data processing constructs contours of constant attenuation rate (phase constant) across the plan view of the panel. In anomalous zones, the contours rapidly change with distance. The shape of the contour lines generates a visual image of the anomaly and suggests the type of anomalous condition to be expected in the coal seam.

This paper briefly discusses the depositional environment and the formation of the imperfect waveguide in coal-bearing strata. The linkage between sedimentary geology and EM wave theory establishes an understanding of how the propagation constants depend on the anomalous geologic conditions. A case study compares in-mine geologic mapping with the tomographic image of a longwall panel.

Introduction

The transformation of mechanized coal-extraction machines

L.G. Stolarczyk, member SME, is Vice President for Research, Stolar Inc., Raton, NM. R.C. Fry is Exploration Administrator, Pacific Corp., Salt Lake City, UT. SME preprint 89-179, SME Annual Meeting, Las Vegas, NV, Feb. 26-March 1, 1989. Manuscript February 1989. Discussion of this paper must be submitted, in duplicate, prior to Sept. 30, 1991.

into semi-automated machines has significantly increased safety and productivity, and the transformation has been combined with improved planning and scheduling to significantly reduce extraction cost. Maintaining the lowest possible cost depends on management and containment of a wide variety of risk factors. Experience and diligence allow us to identify and manage many of these risk factors. However, the risk factor that is least expected or not planned for is the one that is likely to create the greatest disruption in the mining process.

One of the risk factors that has been difficult to plan for in advance of mining is unexpected changes in geology. Often, anomalous seam conditions result in rapidly thinning coal (scours), rock intrusions into the seam (faults, dikes and sills) and changes in the lithology of the surrounding sediment layers (paleochannels).

When the shearing drums cut into rock, flying sparks can cause methane and coal dust ignitions. Out-of-seam rock decreases run-of-mine (ROM) coal quality. Silica in the dust makes it difficult to comply with MSHA respirable dust regulations. Cutting into rock increases wear and tear on the cutting drum and mechanical components of the shearer or continuous miner. This leads to additional maintenance and down time.

Mine personnel must work long hours in difficult circumstances to mine through disturbance zones. Mining costs escalate and morale may fall in the organization.

The first step taken to reduce geologic-risk was to improve the geologic data base by increased core drilling and geologic mapping along the entries in the mine. Stratigraphic cross sections and plan-view maps of the paleochannel flow improved the reliability of forecasting of difficult mining conditions. However, while these techniques identified anomalous zones, the threat to mining in a longwall panel could not be determined to a confidence level acceptable for realistic mine planning.

The next step was to search for reliable and cost effective diagnostic imaging technology that could determine geologic structure in advance of mining. A breakthrough in diagnostic imaging technology occurred when the coal seam waveguide was discovered during the field test and evaluation of the US Bureau of Mines (USBM) medium frequency radio system. Radio communications range in the coal seam waveguide exceeded 210 m (700 ft). This long range suggested that a "medical CAT scan" technology might be developed to image geologic structure in 150 m x 1600 m (500 ft x 5280 ft) longwall panels.

Several technical issues arise in accessing the validity of applying radio waves in diagnostic imaging applications. Tomography algorithms developed in the early 1980s required that the EM wave travel along straight ray paths in the waveguide. Waves that bounce between the roof and floor sediment layers or follow curved (diffracted) paths cannot be processed accurately to determine the propagation constants. To be sensitive to

changing seam conditions, the radio wave propagation constants must be strongly dependent upon the seam height and lithology of the sediment layers. Rapid changes in seam height of the order of 0.3 m (1 ft) can cause shearing machine clearance problems in 2.1-m (7-ft) seams. Along margins of paleochannels, fractured roof causes longwall roof support problems. The long wavelength [152 m (500 ft)] of radio wave in the seam creates image resolution concerns. The resolution may not be good enough to detect a 3-m (10-ft) washout.

To answer these issues, knowledge and experience from EM wave theory, sedimentary geology and mining engineering had to be brought together in the context of the diagnostic imaging problem.

In the context of the underground seam wave communications problem, Wait (1976) formulated the seam wave problem and determined the values of the propagation constants in a uniform seam. In reviewing Wait's results, it appeared that the seam wave would be highly responsive to changing seam conditions.

It is interesting to note that Wait (1963) had already envisioned the existence of natural waveguides in the earth. Wait believed that radio waves propagating in the earth's natural waveguides could provide communications between highly sensitive military installations that would be virtually impossible to destroy in a nuclear attack. The top of the waveguide was expected to be the high conductivity (0.1 S/m) upper crust of the earth overlying a lower conductivity (10^{-5} S/m) granite layer. The bottom of the waveguide was assumed to be the underlying thermal region of the earth.

DeBettencourt and Taso (1963) demonstrated 1830 m (6000 ft) of crosshole radio signalling range at 100 and 4200 Hz. Distances of greater than 12,200 m (40,000 ft) were achieved in related tests in a New Mexico potash seam. Following the "rediscovery" of the coal seam wave in USBM radio communications work, Wait (1976) defined the coal seam wave propagation theory illustrated in Fig. 1.

Radio wave energy propagation occurs in the seam because the higher conductivity sediment layers surrounding the seam force the radio wave energy to flow in the coal seam between the sediment layers. A smaller amount of energy escapes through imperfectly conducting sediment layers. Energy is also dissipated as heat in the seam layer. The electric (E) field component of the EM wave is polarized between the mudstone and claystone sediment layers. There is a small electric field component (E_x) aligned in the direction of propagation. The magnetic (H) field

component is directed into the page. The horizontal magnetic field is transverse (TM) to the plane containing the vertical radiating (Tx) and receiving (Rx) loop antennas.

Because the seam height is small compared to the wavelength, only cylindrically spreading zero order mode transverse electromagnetic (TEM) waves propagate in the waveguide. Higher order modes quickly vanish with distance from the radiating antenna. This means that the magnitude of the seam wave is constant across the height of the waveguide. If higher order modes could exist in the waveguide, the magnitude of the fields would vary with seam height.

The seam wave energy travels along a straight ray path(s) and does not bounce from floor to roof layer boundary - like a seismic seam wave. Wait's work establishes the validity of the straight ray assumption used in tomography.

In the context of the radio communications problem, DeLonge (1982) determined the seam wave attenuation rate for a few seam and boundary layer conditions. Hill (1984) of the US National Institute of Standards and Technology in Boulder, Colorado formulated the seam wave problem and investigated tomographic inversion of the measured coal seam data. Hill provided families of curves that related the seam wave propagation constants to the geologic electrical parameters of the seam (seam height and the conductivity of the coal and the rock). His results will be described in this paper.

The strong propagation constant dependence on the thickness and conductivity of the sediment layers resolved the sensitivity issue. Hill (1986), Shope, Greenfield and Stolarczyk (1986) and Shope (1988) consider the theoretical problem of wave propagation in a uniform seam. EM wave propagation in seams with anomalous geologic conditions are currently being investigated in research programs sponsored by the Australian Coal Industry Research Laboratory (ACIRL). Dr. Keeva Vozoff of McQuarie University is leading the research in this area. Dr. Roy Greenfield and graduate students at Penn State University are also working in this area.

Recognizing the imaging possibility of the seam wave, Stolarczyk (1984, 1986) developed instrumentation and survey methods to determine seam continuity and image anomalous geologic structure in advance of mining. Field trials and practical application of the seam wave tomography were required to investigate the resolution and mining issues. The first survey was carried out in Utah Power and Light Company (UP&L) mines in central Utah (1985, 1986).

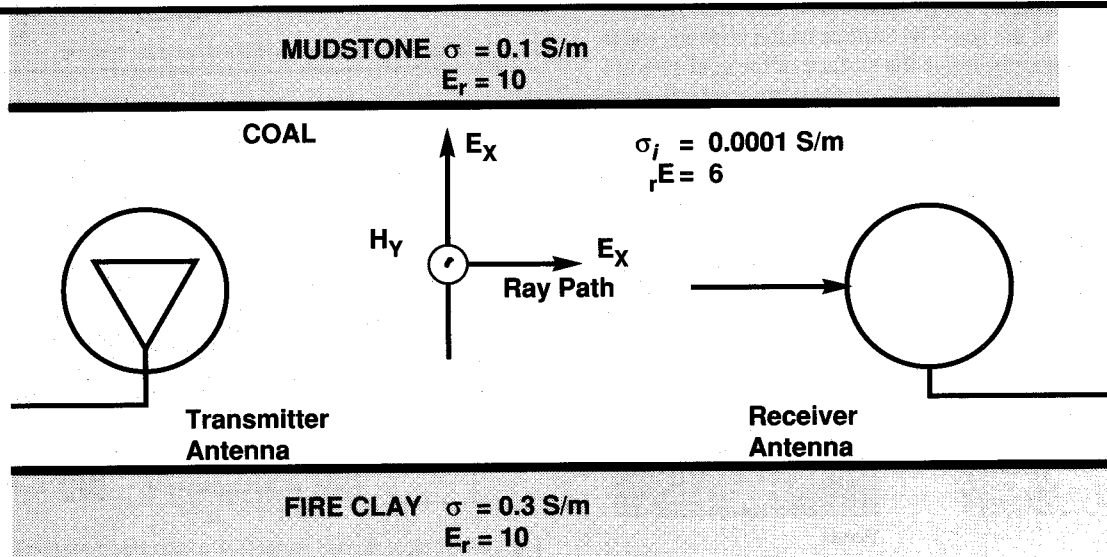


Fig. 1—Cross section of a coal seam illustrating radiating (Tx) and receiving (Rx) magnetic dipole loop antenna.

The tomographic image and in-mine geologic mapping in the Utah mines determined that rapidly thinning coal zones could be detected from RIM scanning between gate roads of a longwall panel. Thinning seams (scours) down to about 0.3 m (1 ft) were accurately predicted from the measured data. Spars with diameters of less than 6.1 m (20 ft) were also detected.

Concurrent investigations were also carried out in Raton Coal Basin mines near Raton, New Mexico and the Orchard Valley Mine near Penosa, Colorado. Seam waves reacted strongly to faults in these seams.

Extensive applications of in-mine and down-hole RIM technology were conducted in Southern Ohio Coal Co. mines (1986). Field tests and subsequent mining proved that paleochannels could be detected and mapped in the mining reserve.

Similar investigations were carried out in New Zealand (1987), Australia (1988), South Africa and the United Kingdom. The field and technical work established the linkage between geology, mining and EM wave propagation theory. The strength and weaknesses of the new technology was accessed in these investigations.

Linkage between coal-seam geology and EM wave propagation theory

The interpretation of the measured data and tomography images requires a knowledge base that includes the depositional environment, formation and alteration of the natural waveguide, and the dependence of the seam wave propagation constants on the electrical parameters of the waveguide. Geologists and mining engineers have developed depositional models that attempt to explain how a deposit was formed and altered throughout geologic history. Predominant geologic anomalies in natural waveguides, including dikes, sills, faults, interbedding and fluvial sandstones (mudstone fill) channels, are illustrated in Fig. 2.

Martin (1896) and Ward (1984) describe a number of different types of environments that fostered vegetation and were subsequently covered by sedimentary deposits. Deltaic coal depositional models are useful in illustrating the formation of natural waveguides and geologic disturbance zones illustrated in Fig. 2. Deltaic peat coal swamps were formed adjacent to ancient river distributaries that flowed into the sea as illustrated in Fig. 3.

Throughout the delta-formation period, sand and mud levees were built up to guide the many distributary channels through the swamp region to the sea. The surface of the channel water was often several meters above the surface of the coal swamp. The changing depositional environment exerted a great influence

on the electrical conductivity of the coal seam and surrounding sediment layers. Often, resistivity logs show that the seam floor sediment layer is highly conductive ($\sigma > 0.1$ S/m).

Typically, floor rock sediments were deposited at or near the strand line of the marine environment. As a result, sediments are either fine or medium grained, well sorted sand or interdistributary mudstone deposited in brackish water. In any case, these rocks normally display characteristics of their brackish water depositional environment. The floor sediment rock contains precipitates usually in the form of sulfites. When saturated with water, the salts become ionized increasing the electrical conductivity to above 0.1 S/m.

The sediments deposited above the coal seam occur in a fresh water environment, relatively free from the salts present in the near marine environment. The sediments may range from mudstone deposits (interdistributary mud flats) to sandstone (fluvial channel deposits). These sediments normally have much lower conductivity than the floor sediment layer. Mudstone and shale roof sediments are impermeable and restrict injection of water into the seam from overlying aquifers.

Meandering channels can erode through the roof sediment layer and contact the coal seam. Fig. 4 illustrates the cross section of a paleochannel contacting the coal seam.

Often, the energy level of the water in meandering channels is sufficiently high to cause erosion or scour the mudstone above the coal and the peat coal itself. An overlying sandstone aquifer can inject water into the coal seam causing the electrical conductivity of the local zone of the seam to increase. The

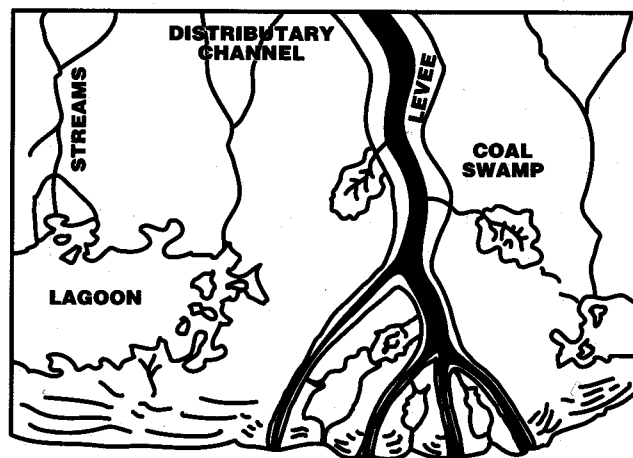


Fig. 3—Delta region of an ancient peat coal swamp.

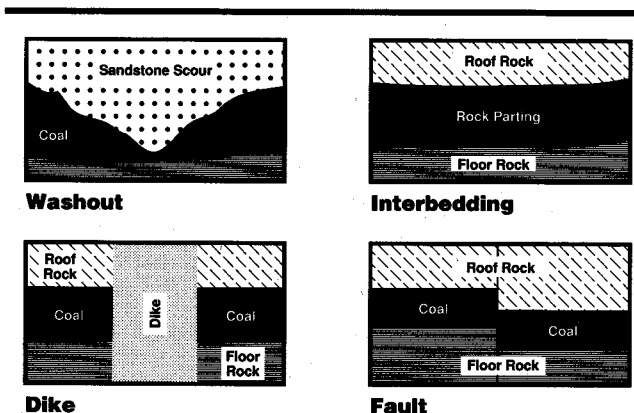


Fig. 2—Natural waveguide anomalies.

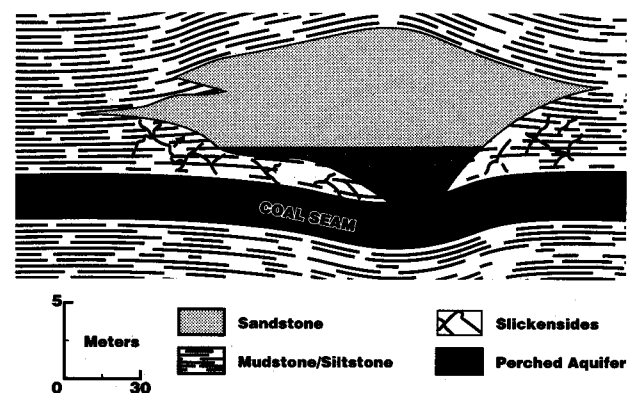


Fig. 4—Vertical across section in a layered formation illustrating a fluvial sandstone channel (sketch by John Mercier of Cypress Minerals).

injection depends upon the porosity and permeability of the sandstone channel. Some channels are filled with mudstone. An unusual channel was filled with rock boulders.

The overlying lenticular sandstone member is less compressible, and the weight from the overlying sediments causes the sandstone layer to press into the more compressible layers. Differential compaction in the surrounding layers and coal seam causes the immediate overlying sediment layer to undergo stress. This produces fractured rock as indicated by the slickensides in the roof rock fragments. Mining under the channel margins exposes the mining process and mine personnel to the risk of rock fall.

Adjacent to the sandstone channels, small fractures sometimes occur in the seam. When the fractures are filled with sandstone or clay, they are called spars. If the underlying sediment layer is relatively soft, the weight of the channel can cause lateral flow in floor sediment. The floor sediments push up into the seam causing "horse backs." The "horse backs" occur 15 to 30 m (50 to 100 ft) away from the margin of the channel. EM waves strongly react to the effect of paleochannels on the seam waveguide. Spars and horse backs produce relatively weak response in the EM wave.

In coal basins with volcanic activity, vertical dikes and sills are normally found in the coal seam. Thin dikes are sometimes filled with soft claystone. However, thicker dikes and sills are

often extremely hard rock. In the Raton seam of northern New Mexico, sills have replaced the coal. Seams in Australia and South Africa have dikes and sills that create severe mining problems.

It is common to find areas in the coal seam where a rock parting is present. Often, parting is formed by a breach in the natural levee. As mentioned above, breaches produce scouring in the peat/coal. The turbid channel water flow into the swamp reacts with acidic water in the swamp causing flocculation of the sediment load. The "middlemen" band thickness in the coal seams can rapidly change.

In many coal bearing formations, tectonic activity and differential compaction can cause faults to occur in the seam. Often, faults occur contemporaneously with the deposition of the roof sediment layer. Faults of this type result in localized seam displacement.

Seam waves propagating in uniform waveguides interact with the geology in predictable ways. The wave propagation constants can be theoretically determined from Hill's work and measured in the coal seam. The close comparison of theoretical and measured values confirms the validity of the theoretical formulation. Hill's work will be described in the following paragraphs to establish the linkage between waveguide geology and seam wave theory.

Radio waves propagating along path(s) in the coal seam are illustrated in Fig. 5.

The sinusoidal radio wave is illustrated in Fig. 6. The notion of radio signal attenuation rate is seen in the value of the receiving antenna output voltage at the transmitter and receiver locations. Coal seam attenuation decreases the magnitude of the radio signal along the path. The phase of the radio signal is shifted by (θ) electrical degrees. Since the ray path distance (r) between antennas is known, the attenuation rate (α) in decibels (dB) per 30 m (100 ft) can be determined from the measured data. The phase shift (θ) in electrical degrees along the ray path(s) can also be measured at the receiver location with RIM System II instrumentation. The phase shift ($r\beta$) is the product of the phase constant (β) and the ray path distance (r). The measured phase is used to determine the average phase constant along the ray path. The wavelength is the distance traveled on the ray path that results in 360° of phase shift.

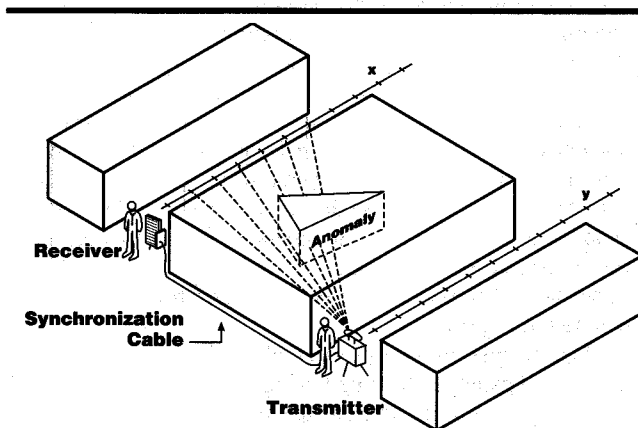


Fig. 5—Sinusoidal radio wave signal paths in a coal seam.

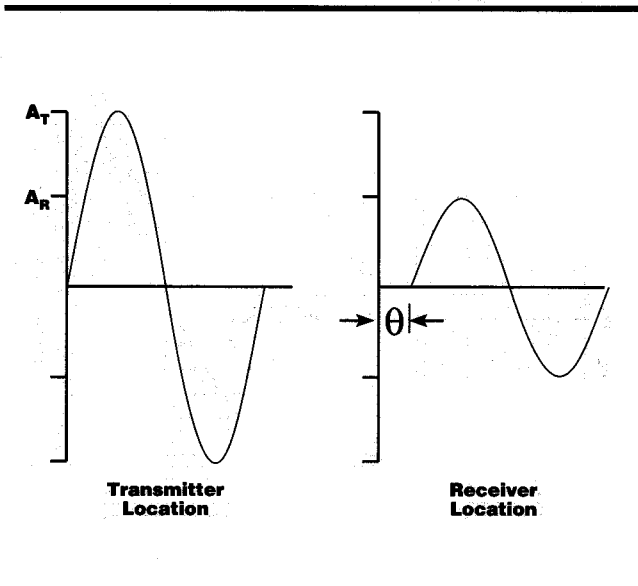


Fig. 6—Sinusoidal radio wave signals along a ray path.

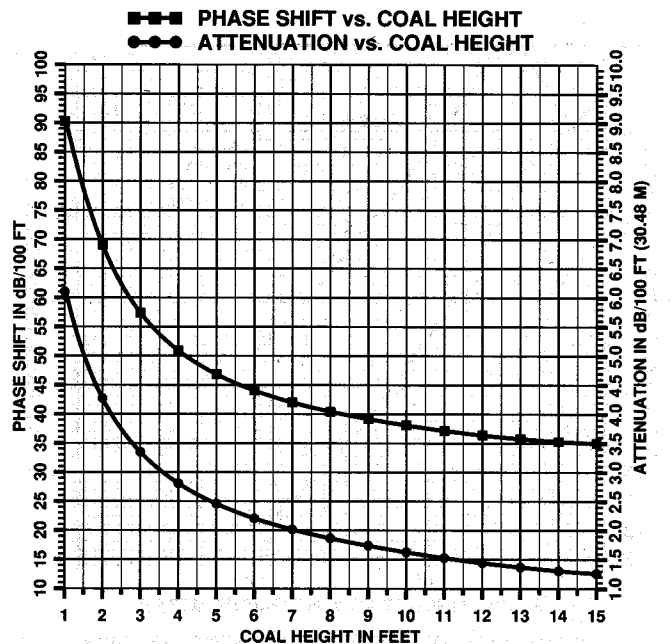


Fig. 7—Attenuation rate and phase shift vs. seam height.

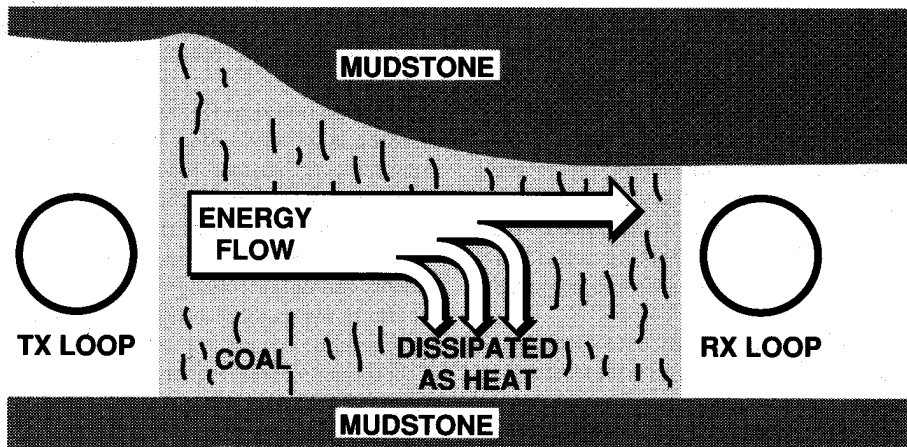


Fig. 8—Energy flow along the ray path from the radiating (Tx) to Receiving (Rx) antenna.

The attenuation rate and phase constant dependence on seam height (h) is illustrated in Fig. 7.

The curves suggest that the propagation constant values are inversely related to seam height. The propagation constants are expected to increase in rapidly thinning coal zones in the panel. The seam wave is expected to produce strong response to scouring in the panel.

The increase in attenuation rate can be explained from an EM wave energy flow point of view in Fig. 8.

When the seam height decreases, the energy density per square centimeter of coal increases. Heating increases the dissipation of the radio wave per unit of travel distance.

The propagation constants increase with decreasing conductivity of the surrounding sediment layers as illustrated in Fig. 9.

The propagation constants increase when the roof/floor lithology changes from mudstone (0.1 S/m) to lower conductivity sandstone (0.01 S/m).

The sandstone contact zone allows the electrical conductivity of the disturbed roof sediment layers to decrease. Energy leaks from the waveguide into the surrounding strata.

The propagation constants increase with the conductivity of the seam as illustrated in Fig. 10.

The propagation constants are highly dependent on seam conductivity. The coal seam electrical conductivity depends upon a number of factors relating to the depositional environment, subsequent alteration, age and rank of the coal. The argillaceous nature of the seam caused the conductivity of the seam to increase with inherent or induced moisture. Coal seams with higher methane gas concentrations are frequently quite dry. Low moisture bituminous coals have conductivity near 104 S/m.

Seam anomalies cause local regions of the coal seam conductivity to increase and become highly responsive targets. Faults and shear zones allow water to be injected into the coal seam. The conductivity of the coal appears to increase for tens of meters, creating a larger target in the coal seam. Rock parting can form a moisture barrier in the coal seam. This increases the conductivity of the coal above the layer. Dikes and sills burn the contact zone of the seams. The attenuation rate measured in different coal seams is indicated in Table 1.

The maximum path distance can be determined from the data illustrated in Fig. 11.

RIM transmission surveys are conducted between gate roads of a longwall panel as illustrated in Fig. 5. The measured data is processed to determine the change in propagation constants

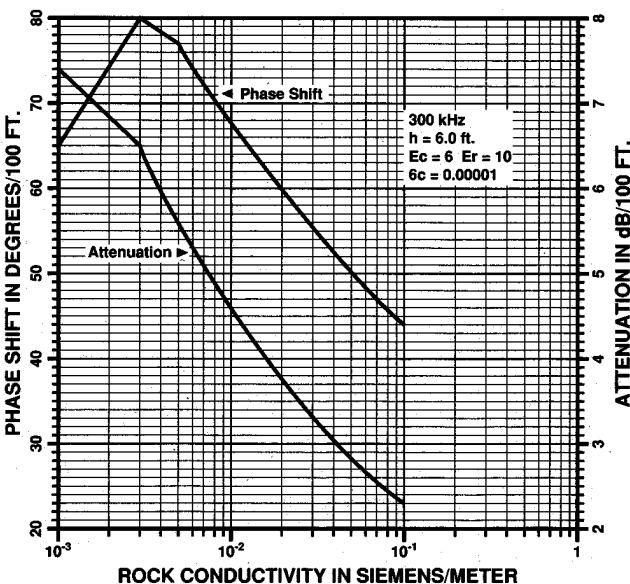


Fig. 9—Seam wave propagation constant values vs. surrounding sediment layer conductivity (after Hill [1984]).

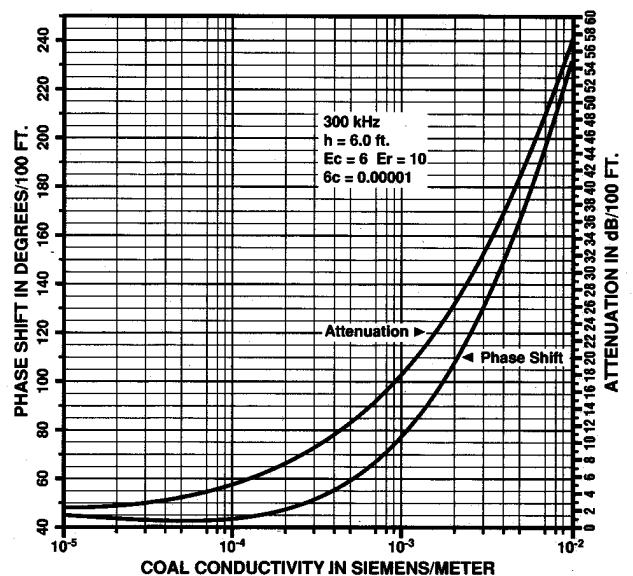


Fig. 10—Seam wave propagation constant values vs. seam conductivity (after Hill [1984]).

Seam	Height		Attenuation rate dB/100 ft
	m	(ft)	
Blue Creek, Alabama	2.1	(7)	3 dB
Bulli, NSW, Australia	2.5	(8.2)	4 dB
Pittsburgh, West Virginia	2.1	(7)	5 dB
Blind Canyon, Utah	2.7	(9)	8 dB
Clarion 4A, Ohio	1.8	(6)	7 dB
New Denmark, S.A.	2.7	(9)	8 dB

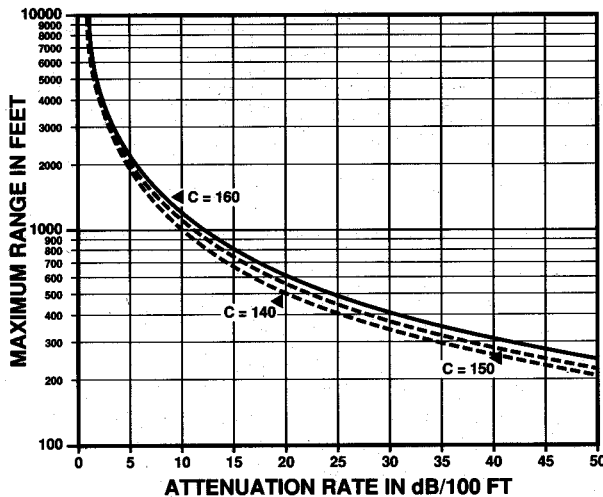


Fig. 11—Maximum system operating range vs. seam wave attenuation rate for system coupling constants of 140, 150 and 160 re 1 nV.

across the plan view of the panel. A typical transmission survey of a panel along with measuring stations is illustrated in Fig. 12. The ribs of the panel are marked in 15-m (50-ft) intervals. The

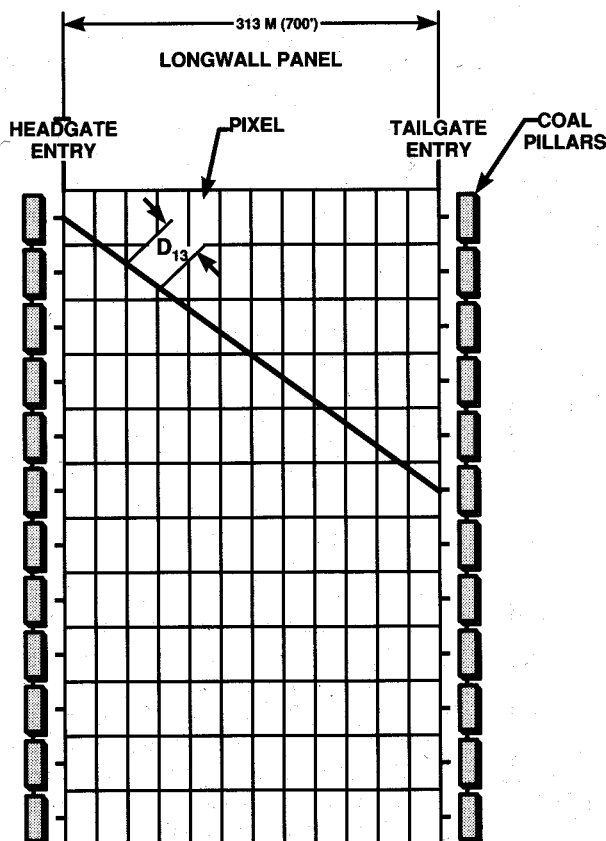


Fig. 12—Plan view of a longwall panel illustrating measuring stations, the K th ray path, and tomography pixels.

transmitter is located at a measuring station. The transmitter is turned on, and the K th path radio wave magnitude and phase are measured at the receiver measuring stations. A grid covering the panel is established by drawing horizontal lines connecting points midway between the measuring stations. Vertical lines are drawn creating the boundaries of the pixels. Since the total signal path attenuation (L_k) and path distance is known along each ray path, an average rate in each pixel along the path can be determined from the measured data set. The measured data set is processed by an iterative reconstruction algorithm. Dines and Lytle (1979) describe an algorithm that can be used to process the data. Since the K th ray distance (d_{ijk}) through each pixel is known, the average attenuation rate (α_{ij}) in each pixel can be determined from the total attenuation (L_k) measured on the K th path as:

$$L_k = \sum_{i=1}^I \sum_{j=1}^J \alpha_{ij} d_{ijk}$$

The iterative process solves K linear equation in IJ unknowns. The average value of α_{ij} is determined from the set of measured L_k . The summation in the above equation is over all values of I and J where $d_{ijk} = 0$ in pixels not intersected by the K th ray path. Because of the length and width of the pixel dimensions vary, the number of equations is usually insufficient to determine all uniquely. As a result, the set of linear equations is over or under determined. Instead of direct matrix conversion, iterative solutions are used to determine α_{ij} . The Algebraic Reconstruction Technique (ART) treats one equation at a time. ART changes the pixel values found in processing each ray path data. Simultaneous Iterative Reconstruction Techniques (SIRT) change the pixels after processing all paths.

The iterative process begins with an initial guess of the pixel value (attenuation rate or phase constant). Multiple iterations routinely modify the pixel values until the ray path signals synthetically determined from the pixels is within a few percent of the measured data set. The set of pixel values represents the propagation constant model for the panel. A contouring algorithm (Golden Software) is used to generate contours of constant pixel value curves in the image plane.

The family of contour lines provides a visual image of the anomalous geologic structure in the seam. The general shape of the image when combined with in-mine geologic mapping in the gate entries can often be used to identify the type of anomaly in

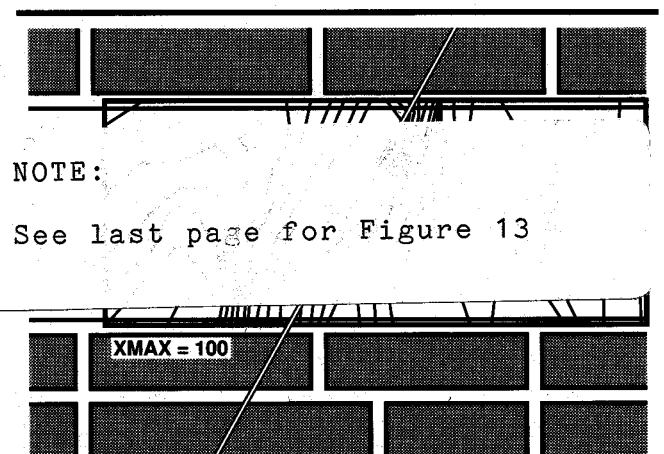


Fig. 13—Plan view of a longwall panel with paleochannel scouring in the headgate and tailgate entries. Tomography image illustrates the contours of constant attenuation rate overlying the panel.

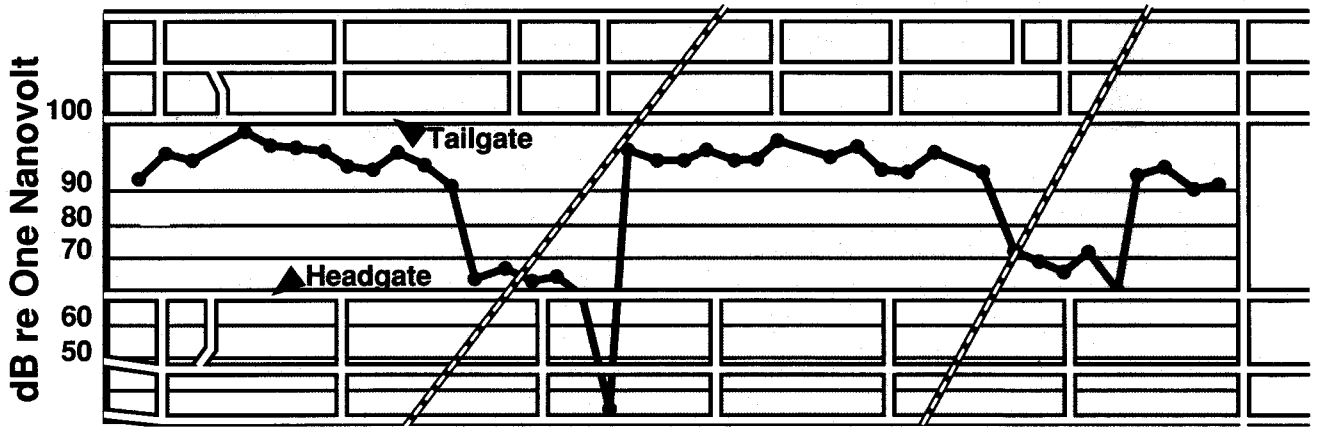


Fig. 14—Plan view of a narrow panel intersected by dikes. The received signal levels (dB re 1 nV) measured on direct paths at each gate measuring station are indicated by dot symbols.

the panel. Although the identification is important, the assessment of the threat in mining requires that the pixel values be related to the geology. Hill's research work is important in establishing the linkage between pixel values and variations in seam height (scouring), changes in roof/floor lithology (sediment layer conductivity) and seam conductivity (rank or interbedding).

RIM EM wave tomographic imaging results

The reconstructed tomography image of a paleochannel washout zone in a longwall panel is illustrated in Fig. 13. The image also shows the headgate and tailgate entries developed for a 600 ft-wide retreating longwall.

The tomography image shows the constant attenuation rate contours determined from processing RIM tomographic scan survey data. The higher than normal attenuation rates are apparent in the headgate and tailgate entries. The higher rates were caused by a channel scour (thin coal). The high attenuation

rates on the tailgate side of the panel between measuring stations 1300 and 1500 were also caused by a channel scour. The seam height was reduced from 2.4 m (8 ft) to 1 m (3 ft) in the scour. The scour was severe enough to suggest that the longwall be terminated at headgate measuring station 1600. Termination of the longwall was a problem because the next panel would not be ready for production and the longwall would be forced to stand idle. The tomography image suggested that the scours were local and the center of the panel would be free of scours. The longwall mined through the disturbance zone and recovered 100,000 st of coal.

The margins of an ancient river channel in the roof are outlined by the rapid increase in attenuation (high gradient). The inby margin crosses the panel between the 1700 headgate and 1600 tailgate measuring stations. The outby margin crosses the panel between the 1300 headgate and 1100 tailgate measuring stations. Differential compaction has caused the roof rock to fracture along the margins of the paleochannel as illustrated in the vertical cross-section of the geologic zone in Fig. 4. The

margins suggest where bad roof rock conditions occur in the panel. From a worldwide coal mining perspective, roof falls are a leading cause of injuries.

EM waves interact strongly with dikes as illustrated in Fig. 14. The direct ray reconnaissance scan results show that the measured signal level drops by approximately 30 dB when the ray paths intersect the dike. The attenuation rate is almost constant along the dike suggesting that the dike thickness remains constant. This interpretation is consistent with in-mine geologic mapping of the exposed dike.

Fig. 15 is the tomographic diagnostic image of a fault crossing a developed longwall panel.

The increased gradient in the contour lines indicates the margins of the geologically disturbed zone caused by a 2.1-m (7-ft) displacement fault. The reconstructed image shows that the fault trends from the upper right to lower left side of the image. A full seam displacement fault is found in the headgate entry while two 0.9-m (3-ft) displacement faults appear in the tailgate entry. A fault will continue along the dashed line

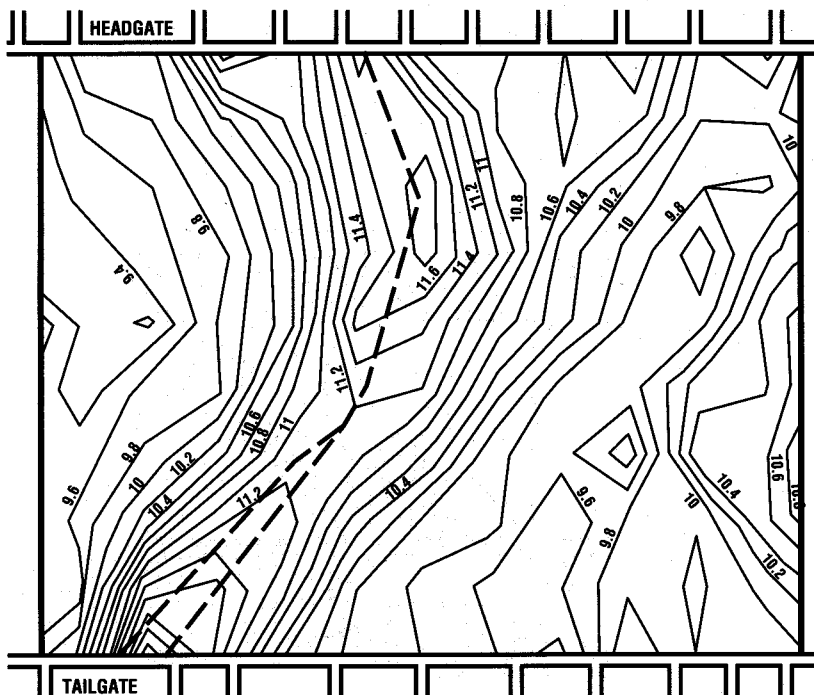


Fig 15—Plan view of a longwall panel with a 1.2-m (7-ft) displacement fault in the headgate entry and split faults in the tailgate entry.

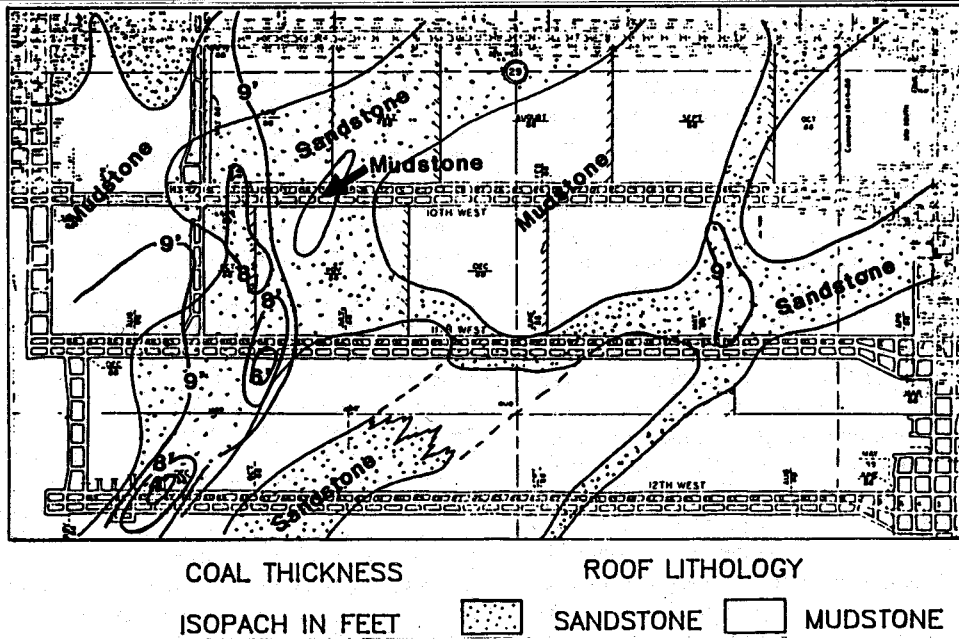


Fig. 16—Plan view illustrating the in-mine geology map flow over three longwall panels. Seam height and roof lithology were monitored during the longwall mining. The monitored seam height is illustrated by contours of constant seam height.

shown in Fig. 15 to approximately the middle of the panel. Poor roof conditions are expected to extend approximately 30 m (100 ft) on each side of the fault line. A retreating longwall moving toward the fault encountered poor roof conditions approximately 30 m (100 ft) from the fault. Longwall mining was terminated at that location.

Recent RIM diagnostic ray surveys of three adjacent longwall panels in Energy West's Cottonwood Mine in central Utah provided valuable information regarding the characteristics of the coal seam and enclosing strata. The area of the longwall panels contained coal that was expected to range from 2.3 m (7.5 ft) to greater than 3 m (10 ft) in thickness as illustrated in Fig. 16.

The roof lithology was extremely variable with mudstones, carbonaceous mudstone and sandstone. A major north-south trending fluvial system overlay the west end of the longwall panels. Several smaller channel systems trending in an east and northeast direction were present above much of both panels. The characteristics of the

sandstone deposited in the channels indicated that significant scouring of the coal may be present below the channel. The floor lithology is fairly consistent being a thin mudstone layer (less than 0.15 m (0.5 ft)) that overlays a massive marine sandstone.

Previous mining and in-mine geologic mapping experience had shown that areas having similar roof lithology and coal thickness conditions can contain localized areas of thin coal caused by fluvial scours. The potentially adverse effect on production and coal quality was considered serious enough that a diagonal RIM survey was conducted on both panels. The objective of the survey was to identify any area of coal having a thickness of less than 2.1 m (7 ft) that may be present and to gain enough information regarding the coal seam and roof lithology to enable an accurate forecast to be made of the run-of-mine (ROM) coal quality. Normal ash, in a uniform seam, is approximately 12%. It has increased to 17% along the margins of the channel. The panels were surveyed after initial development

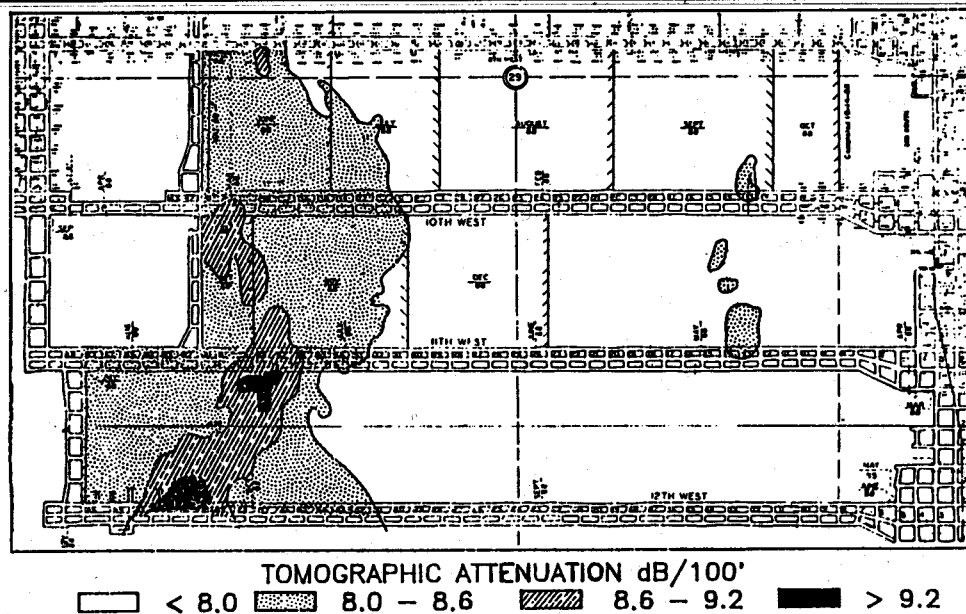


Fig. 17—RIM tomography image illustrating constant attenuation rate zone.

was completed on May 21, 1988 for the 10th west longwall panel and on Oct. 8, 1988 for the 11th west longwall panel.

The measured data was processed in a tomography algorithm. The higher constant attenuation zones in Fig. 17 delineated where the channel systems cross above the two longwall panels.

The western 300 m (1000 ft) of the panels contained conditions that caused higher attenuation of the EM seam wave signal when surveyed. This was caused by the overlying sandstone channel that was mapped in the entries. The data indicated that the main channel actually has two branches that are separated by a mudstone layer in the roof. At several locations within the channel area, higher attenuation rates were computed in the diagnostic tomographic algorithm. These local areas were interpreted as minor scouring of the coal seam by the overlying fluvial system. Our interpretation indicated that the thinning of the coal was not severe enough to seriously effect the longwall production or ROM coal quality. Therefore, the longwall mining was undertaken through these areas as planned rather than avoiding them by driving new set-up eateries. As longwall retreated through these areas, local thinning zones were indeed found, which confirmed the original interpretation. The central 600 m (2,000 ft) of the panel was dominated by mudstone roof rock. No mining problems were anticipated from the reconstructed tomographic image. This was also confirmed by mining.

A channel was also identified in geologic and RIM tomographic data. The RIM tomographic data indicated a fluvial sandstone was present in the tailgate side of the 11th west panel. Mining progressed through the area and exposed the scour. The location and geometry of the scour coincides with the increased attenuation rate contours on the reconstructed tomographic image.

Summary

RIM tomographic images have been compared to in-mine geology mapping acquired when mining through four different longwall panels. The images have proven reliable in mapping paleochannels across a longwall panel. Local zones of thin coal have been accurately appeared as forecast in the image. Seam height changes of approximately 0.3 m (1 ft) have been detected in the image. The tomography images proved to be accurate and of significant value in the understanding of the prevailing geology.

References

- DeBettencourt, J.T., and Tsao, C.H.K., 1963, "Measurement of Phase Constant for Rock Propagated Radio Signals," *IEEE Transcript on Communications Technology*; August.
- DeLonge, P., 1982, "Leaky Feeders and Subsurface Radio Communications," *IEEE Electromagnetic Wave Series 14*, Peter Peregrinus, Ltd., Stevenage, U.K.
- Gumbley, J., Stolarczyk, L.G., and Shope, S., 1987, "The Radio Imaging Method (RIM) Evaluation of Longwall Panels in the East Huntley Coal Mine," Fifth Conference and Exhibition, Australian Society of Exploration Geophysics, Perth; February.
- Houghton, S.H., 1960, "The Geology of Some Ore Deposits in Southern Africa," *Geological Society of South Africa*, Vol. 1, Johannesburg.
- Hill, D., 1984, "Radio Propagation in a Coal Seam and the Inverse Problem," *Journal of Research*, National Bureau of Standards, Vol. 89, No. 5, Sept.-Oct.
- Hislop, J., 1985, "Productivity and Profitability at Wilberg Mine," Mining 85—International Mining Conference, Birmingham, U.K.
- King, R.W.P., and Prasad, S.M., 1986, *Fundamental Electromagnetic Theory and Applications*, Prentice-Hall, Inc., Englewood, NJ
- Lloyd, T.W., Semborski, C.A., and Stolarczyk, L.G., 1986, "A Method of Predicting Coal Seam Discontinuities," SME preprint 86-28, SME Annual Meeting, New Orleans, March.
- Martin, E.A., 1986, "The story of a piece of coal," McGiure, Phillips and Co., New York.
- Miller, D., Doe, S., and Stolarczyk, L.G., 1986, "Evaluation of Buried Coal Seam Discontinuities," SME Annual Meeting, New Orleans, March.
- North, F.K., 1985, *Petroleum Geology*, Allen and Unwin, Boston, Mass.
- Ramo, S., Whinnery, J.R., and VanDuzer, T., 1965, "Fields and Waves in Communication Electronics," John Wiley and Sons, New York, pp. 379-383
- Shope, S.M., 1987, "Electromagnetic Coal Seam Tomography," Ph.D. dissertation, Pennsylvania State University, p. 292.
- Shope, S.M., Greenfield, R.J., and Stolarczyk, L.G., 1986, "Use of Electromagnetic Waves for Coal Seam Tomography," *Proceedings, Society for Exploration Geophysics, 56th Annual Meeting*, Houston, TX.
- Sommerfeld, A., 1929, "Über die Austretung der Wellen in der Drahtlosen Telegraphie," *Ann. Physik*, Ser. 4, Vol. 81, No. 17, Dec., pp 1135-1153.
- Stolarczyk, L.G., 1986, US Patent No. 4,577,153, "Continuous Wave Medium Frequency Signal Transmission Survey Procedures for Imaging Structures in Coal Seams," March.
- Stolarczyk, L.G., Rogers, G., and Hatherly, P., 1988, "Comparison of Radio Imaging Method (RIM) Electromagnetic wave tomography with in-mine geologic mapping in the Liddel, Bulli, and Wongawilli Seams," Sixth Conference and Exhibition, Australian Society of Exploration Geophysics, Adelaide, Vol. 19, No. 1/2, March/June, pp. 169-170.
- Stolarczyk, L.G., US Patent No. 4,691,166, "Continuous Wave (CW) Electromagnetic Instruments for Imaging Structures in Geologic Formations (apparatus)."
- Wait, J.R., 1963, "The Possibility of Guided Electromagnetic Waves in the Earth's Crust," *IEEE Transcript on Ant and Prop*, Vol. AP-1, No. 3, May.
- Wait, J.R., 1963, *IEEE Transcript on Ant and Prop*, Vol. AP-1, No. 3, May.
- Ward, C.R., 1984, *Coal Geology and Coal Technology*, Brackwell Scientific Publications, Palo Alto, CA.
- Wattley, G., 1988, "Follow-up Report of Management and Procurements of Fuel and Property Policies and Practises," Southern Ohio Coal Company Public Service Commission Audit, Arthur D. Little case number 88/101/EL/EFC, p. 24. August.

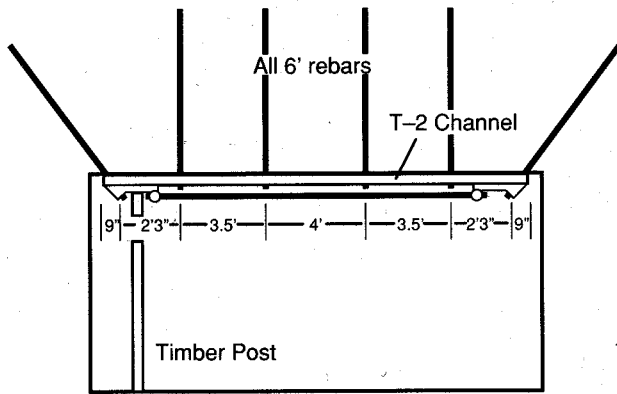


Fig. 10—Modified roof reinforcement system, primary bolting and truss bolts are installed in cycle and timber post positioned under the cutter.

tension and one 2.4-m (8-ft) torque tension bolts, two 3.6-m (12-ft) superbolts, a truss bolt and a yieldable post at the cutter side. In both cases, an additional yieldable post was set near the center of the entry following the advance of belt conveyor feeder (Fig. 9). Furthermore, installation time and labor for truss and steel beams were almost the same (six trusses per shift for crew of two while 10 beams per shift for crew of four).

The cost for 1.5 m (5 ft) of roof support for the new method was \$265.21 or \$16.07/m (\$53.04 per ft) of entry development. Despite more than 17% cost savings, the new method stabilized the roof strata and eliminated the need to reestablish roof support during longwall face retreat, hence improving the rate of advance of longwall retreat mining through time saving.

The cost of entry development was reduced to \$5.10 and \$8.50/m (\$16.86 per ft and \$28.10 per ft) for 1.5 m and 0.9 m (5 ft and 3 ft) spacing, respectively.

Conclusions

Due to high in situ stresses and bad roof conditions, implementation of yield pillar could not eliminate the development of the cutter roof in this mine. Furthermore, due to the highly laminated condition of the roof strata, yield pillar design was found to be ineffective concerning stability of entries. However, roof reinforcement through proper reinforcement design and time of application were found to

Correction

In the 1990 Transactions paper "Radio imaging method (RIM) for diagnostic imaging of anomalous geologic structures in coal seam waveguides" by L.G. Stolarczyk and R.C. Fry, figure thirteen should have been presented as follows:

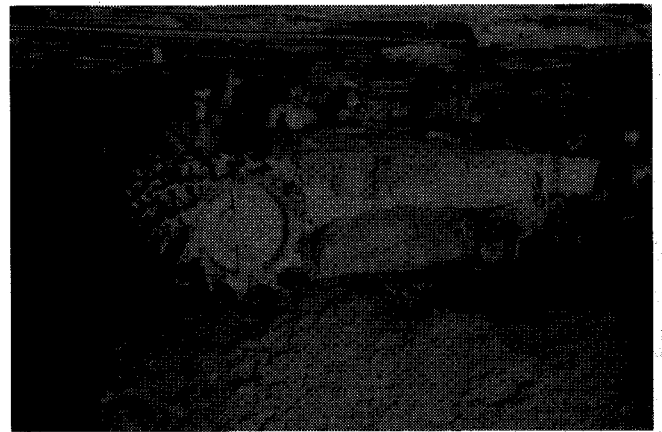


Fig. 11—Entry supported with modified reinforcement system.

be very effective. In this mine, the cost of associated materials for roof reinforcement was reduced to one-fourth of the old system in addition to improving the rate of advance of both panel entries and longwall retreat mining.

Acknowledgment

This project was co-sponsored by Beth Energy Mines Inc. and West Virginia University's Energy and Water Research Center and the College of Mineral and Energy Resources. The writers acknowledge assistance of Danqing Xu, research assistant at the Mining Engineering Department of West Virginia University in the preparation of this paper.

References

- Iannacchione, A. T., and D. G. Puglio, 1979, "Geology of the Lower Kittanning Coalbed and Related Mining and Methane Emission Problems in Cambria County, PA," US Bureau of Mines RI 8354, 31 pp.
- Watson, B., 1979, "Longwall Produces Record Tonnage," *Coal Age*, Vol. 76, No. 3, pp. 64-75.
- Hooker, V. E., Bickel, D. L., and Johnson, C. F., 1969, "Near Surface Horizontal Stresses Including the Effect of Rock Anisotropy," US Bureau of Mines RI 7224, 29 pp.
- Bickel, D. L., and Donato, D. A., 1988, "In situ Horizontal Stress Determinations in the Yampa Coalfield, Northwestern Colorado," US Bureau of Mines, RI 9149, 43 pp.
- Wilson, A. H., 1977, "The Effect of Yield Zones on the Control of Ground," *Proceedings, 6th International Strata Control Convergence, Braniff, Canada, Paper No. I-3*, pp. 1-25.

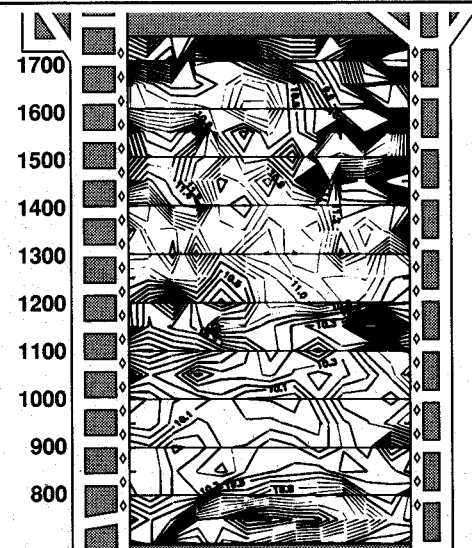


Fig. 13—Plan view of a longwall panel with paleochannel scouring in the headgate and tailgate entries. Tomography image illustrates the contours of constant attenuation rate overlying the panel.